Communication

Plasma-Based Reflective Surface for Polarization Conversion

Mirko Magarotto, Luca Schenato, Paola De Carlo, and Antonio-Daniele Capobianco

Abstract— This study analyses, for the first time, the use of reflective surfaces based on magnetized plasmas for polarization conversion. The feasibility of this concept has been assessed via a theoretical model. Moreover, the numerical design of a plasma-based reflective surface is presented. The latter enables linear-to-linear (LP-to-LP) and linear-to-circular polarization (LP-to-CP) conversion over a broad frequency range, from 7.5 to 13 GHz. To this end, the applied magnetic field intensity has to be tunable over 55–140 mT and its direction steerable toward three mutual orthogonal axes. At the same time, the plasma density has to be controlled up to 2×10^{18} m^{-3}. These requirements are consistent with the plasma technology at the state-of-the-art.

Index Terms— Gaseous plasma antennas (GPAs), linear-to-circular (LP-to-CP), linear-to-linear (LP-to-LP), polarization conversion, reflective surfaces.

I. INTRODUCTION

Gaseous plasma antennas (GPAs) are devices in which an ionized gas, namely, plasma, is used to transmit and receive electromagnetic (EM) waves [1]. This class of antennas present unique advantages over their metallic counterpart, given the possibility to control the EM response of the plasma electronically [2]. First, plasma is produced by energizing a neutral gas confined within a dielectric vessel. Namely, the radar cross section of a GPA can be drastically reduced if the electric power to sustain the plasma is turned off and, thus, the main conductive medium fades [3]. This feature is appealing to minimize the mutual interference between several GPAs stacked into an array [4] or if stealth is required [5]. Second, the plasma properties that drive the antenna performance (e.g., density) can be controlled by varying the electric power coupled to the plasma [6], [7]. Thus, it is possible to reconfigure the figures of merit of a GPA, such as radiation pattern [8], [9], operation frequency [10], and polarization [5].

To date, several systems based on metasurfaces have been proposed to control the polarization of an EM wave in terms of both linear-to-linear (LP-to-LP) and linear-to-circular (LP-to-CP) conversion [11]. With this regard, polarization control can be achieved via resonating [12], anisotropic [13], chiral [14], and artificial magnetic

conductor [15] elements, in both the transmission and reflection modes [16]. Notably, LP-to-LP [17] and LP-to-CP [18] ultrawide-band conversions have been demonstrated relying on anisotropic metasurfaces. Reconfigurable metasurfaces have been proposed to integrate various polarization conversions in a single device [19]. Switching between linear polarization (LP) and circular polarization (CP) [20] as well as between right-handed and left-handed CP [21] is feasible by integrating diodes on the elements that constitute the metasurface.

An alternative approach to controlling an EM wave's polarization envisions using magnetized plasmas [22], [23]. Theoretical investigations proved that by varying the plasma properties (e.g., density), it is possible to selectively control the transmission through a magnetized plasma layer of the right-handed or left-handed CP waves [22], as well as transverse electric (TE) or transverse magnetic (TM) waves [23]. At the same time, EM signals can be controlled by relying on plasma-based reflective surfaces [24], [25]. In these devices, the unit cells consist of plasma elements placed on top of a ground plane. For the first time, the present study explores the use of reflective surfaces based on magnetized plasmas for polarization conversion. Specifically, an analytical model and a preliminary design are proposed to prove that this concept enables significant improvements in terms of polarization conversion with respect to the state-of-the-art. Indeed, a single plasma-based reflective surface might allow generic LP-to-LP conversion and LP-to-CP conversion with the possibility of selecting between the right-handed and left-handed CP. To the best of the authors' knowledge, no other solution proposed in the literature enables all these features in the GHz frequency range and for a relative bandwidth larger than 50%. Moreover, the significance of the numerical results presented in this work is strengthened by the assumption of realistic plasma properties compatible with the technology at-the-state-of-the-art [3], [26].

II. METHODOLOGY

The EM response of the plasma is described via its relative permittivity ε_r. Given the usual operation frequencies (i.e., in the GHz range) and plasma properties of GPAs [2], ε_r is formulated according to the cold plasma model where the ions' motion is neglected [27]. ε_r takes the form of a dyadic tensor to account for the anisotropy induced by the magnetostatic field $\boldsymbol{B}_0$ [28]. Without loss of generality, it is practical to express ε_r in a reference frame where the z-axis is aligned with $\boldsymbol{B}_0$

$$\varepsilon_r = \begin{pmatrix} S & -\jmath D & 0 \\ \jmath D & S & 0 \\ 0 & 0 & P \end{pmatrix} \qquad (1)$$

where $\jmath$ is the imaginary unit, and the adimensional parameters S, D, and P read [27]

$$S = 1 - \frac{XU}{U^2 - Y^2}, \quad D = -\frac{XY}{U^2 - Y^2}, \quad P = 1 - \frac{X}{U}. \qquad (2)$$

The relation between plasma properties and the adimensional parameters X, Y, and U follows [27]:

$$X = \frac{\omega_p^2}{\omega^2}, \quad Y = \frac{\omega_c}{\omega}, \quad U = 1 + \jmath \frac{\nu}{\omega} \qquad (3)$$

where ω, ω_p, and ω_c are the operation angular frequency, the plasma frequency, and the cyclotron frequency, respectively, in rad/s. Instead, the parameter ν is the collision frequency in Hz. Here, ω_p, ω_c, and ν depend on the macroscopic plasma parameters according to the following relations [27]:

$$\omega_p = \sqrt{\frac{q^2 n_e}{m \varepsilon_0}}, \quad \omega_c = \frac{q B_0}{m}, \quad \nu = n_0 K (T_e) \tag{4}$$

where q is the elementary charge, m is the electron mass, ε_0 is the vacuum permittivity, n_e is the plasma density in m^{-3}, B_0 is the intensity of the magnetostatic field in T, n_0 is the neutral background density in m^{-3}, and K is a rate constant that depends on the electron temperature T_e. If plasma is produced from argon gas, K reads [29]

$$K = 2.336 \times 10^{-14} T_e^{1.609}$$
$$\times \exp \left(0.0618 \left(\ln T_e \right)^2 - 0.1171 \left(\ln T_e \right)^3 \right) \tag{5}$$

where T_e is expressed in eV. It is worth stressing that ω_p depends on n_e, and ω_c depends on B_0; this means that in a magnetized plasma, the EM response (i.e., the reflection of an incident wave) can be controlled electronically by acting on two macroscopic parameters. Indeed, the plasma density n_e depends on the electric power used to sustain the discharge [10]. At the same time, the intensity of the magnetostatic field B_0 can be varied using electromagnets (e.g., by current-controlled solenoids) [30]. The collision frequency ν is associated with Ohmic losses occurring within the plasma [24] that are proportional to n_0. With this regard, it is worth introducing the neutral gas pressure p_0, which represents an auxiliary parameter more often used to characterize plasma discharges rather than n_0

$$p_0 = k_B T_0 n_0 \tag{6}$$

where k_B is Boltzmann's constant and T_0 is the temperature of the neutral gas. According to the state-of-the-art for plasma discharges, the maximum value of n_e is proportional to p_0 [6], [7].

In an anisotropic medium where ε_r is given by (1), the relation between the components of the electric field reads [27]

$$\begin{pmatrix} S - u^2 \cos^2 \theta & -jD & u^2 \sin \theta \cos \theta \\ jD & S - u^2 & 0 \\ u^2 \sin \theta \cos \theta & 0 & P - u^2 \sin^2 \theta \end{pmatrix} \begin{pmatrix} E_x \\ E_y \\ E_z \end{pmatrix} = 0 \tag{7}$$

where $\boldsymbol{E} = (E_x; \; E_y; \; E_z)$ is the complex electric field vector, θ is the angle between $\boldsymbol{B}_0$ and the wave vector $\boldsymbol{k}$, and u is the refractive index. From (7), the following dispersion relation derives [27]:

$$u^2 = 1 - \frac{X}{Q} \tag{8}$$

where the adimensional parameter Q reads

$$Q = U - \frac{Y^2 \sin^2 \theta}{2 (U - X)} \pm \left[\frac{Y^4 \sin^4 \theta}{4 (U - X)^2} + Y^2 \cos^2 \theta \right]^{0.5}. \tag{9}$$

For a given direction of the wave vector (i.e., for a fixed θ), two values of the refractive index, namely, u_+ and u_-, satisfy the dispersion relation reported in (8), where the subscripts are consistent with the signs used in (9). Thus, two types of waves may exist simultaneously, from now on called *modes* [27]. Specifically, it is possible to identify cutoff and resonance frequencies that delimit each *mode*'s propagation interval (i.e., u almost real). Outside the interval within the cutoff and resonance frequency, the dispersion relation describes an evanescent wave [31]. For clarity, the cutoff occurs at $u = 0$, while the resonance occurs at $u \to \infty$ [27]. For what *mode* + is concerned, ω_p is a cutoff. Instead, *mode* − shows
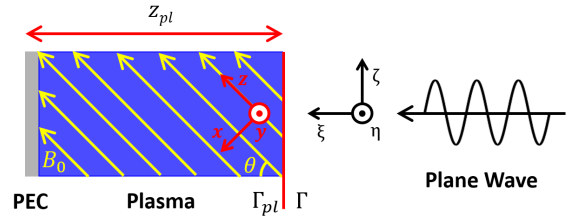

Fig. 1.   Schematic of the plasma element described by the theoretical model.

two cutoffs and one resonance frequency. The cutoffs occur at the following frequencies:

$$\omega_R = 0.5 \left(\omega_c + \sqrt{\omega_c^2 + 4\omega_p^2} \right), \tag{10a}$$

$$\omega_L = 0.5 \left(-\omega_c + \sqrt{\omega_c^2 + 4\omega_p^2} \right) \tag{10b}$$

and the resonance frequency occurs at

$$\omega_0 = \left[0.5 \left(\omega_p^2 + \omega_c^2 \right) + \sqrt{0.25 \left(\omega_p^2 + \omega_c^2 \right)^2 - \omega_p^2 \omega_c^2 \cos^2 \theta} \right]^{0.5}. \tag{11}$$

For what follows, it is more practical to define the propagation intervals in terms of the corresponding plasma density values n_e rather than the operation frequency ω [24]. Specifically, the critical densities n_e^p, n_e^R, n_e^L, and n_e^0 identify the values of n_e for which ω is equal to ω_p, ω_R, ω_L, and ω_0, respectively. Specifically, the *mode* + propagates for $n_e < n_e^p$, while the *mode* − propagates for $n_e < n_e^R$ and $n_e^0 < n_e < n_e^L$. Instead, if $n_e \geq n_e^L$, the plasma behaves as a conductor, namely, only evanescent waves may exist [27].

A. Theoretical Model

A theoretical model has been developed to assess the use of a magnetized plasma as a polarization converter. A schematic of the considered setup is depicted in Fig. 1. A homogeneous plasma slab of thickness z_{pl} is located on top of an infinite perfect electric conductor (PEC), constituting the ground plane [24]. A uniform magnetostatic field $\boldsymbol{B}_0$ is assumed to be aligned with the z-axis of the reference frame depicted in Fig. 1. A linearly polarized plane wave impinges the plasma slab normally. The wave propagates along the ξ-axis, forming an angle θ with $\boldsymbol{B}_0$. The reflected wave is described via the following relation:

$$\boldsymbol{E}_r = \Gamma^+ \boldsymbol{E}_i^+ + \Gamma^- \boldsymbol{E}_i^- \tag{12}$$

where $\boldsymbol{E}_i$ is the complex electric field vector associated with the incident wave, $\boldsymbol{E}_r$ corresponds to the reflected wave, and Γ is the reflection coefficient [24]. As done above, the superscripts refer to *mode* + and *mode* −, respectively. In particular, $\boldsymbol{E}_i^+$ and $\boldsymbol{E}_i^-$ describe the component of the incident electric field which excites the propagation of the *mode* + and *mode* − within the plasma, respectively.

According to the classical transmission line model [31], the reflection coefficient reads

$$\Gamma^{\pm} = \frac{\rho^{\pm} + \Gamma_{pl}^{\pm}}{1 + \rho^{\pm} \Gamma_{pl}^{\pm}} \tag{13}$$

where ρ is Fresnel's reflection coefficient at the air–plasma interface, Γ_{pl} is the reflection coefficient within the plasma medium, and the superscripts refer to the *mode* + and *mode* −, respectively. Fresnel's reflection coefficient reads [31]

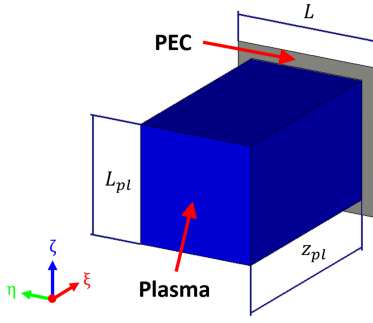$$\rho^{\pm} = \frac{1 - u_{\pm}}{1 + u_{\pm}} \tag{14}$$

Fig. 2. Schematic of the plasma element simulated numerically.

and Γ_{pl} reads [31]

$$\Gamma_{pl}^{\pm} = -\exp\left(j\, 4\pi u_{\pm} \frac{z_{pl}}{\lambda}\right) \tag{15}$$

where $\lambda = c/f$ is the wavelength in air, and c is the speed of light in the vacuum. To separate the $\boldsymbol{E}_i^+$ and $\boldsymbol{E}_i^-$ components, the first step consists of expressing the incident field into the $(x\ y\ z)$ reference frame. Therefore, for geometric construction (see Fig. 1), the following relation holds at the air–plasma interface:

$$\begin{cases} E_y^+ + E_y^- = E_\eta \\ \left(E_z^+ + E_z^-\right)\sin\theta - \left(E_x^+ + E_x^-\right)\cos\theta = E_\zeta. \end{cases} \tag{16}$$

It is worth noting that $E_\xi = 0$ provided that the incident field is a plane wave propagating along the ξ-axis [31]. Using (7), E_η and E_ζ read

$$\begin{pmatrix} -\dfrac{jD}{S - u_+^2} & -\dfrac{jD}{S - u_-^2} \\ -\dfrac{u_+^2 \sin\theta\cos\theta}{P - u_+^2 \sin^2\theta}\sin\theta - \cos\theta & -\dfrac{u_-^2 \sin\theta\cos\theta}{P - u_-^2 \sin^2\theta}\sin\theta - \cos\theta \end{pmatrix}$$
$$\cdot \begin{pmatrix} E_x^+ \\ E_x^- \end{pmatrix} = \begin{pmatrix} E_\eta \\ E_\zeta \end{pmatrix} \tag{17}$$

from which E_x^+ and E_x^- can be calculated. Once E_x^+ and E_x^- are known, the vectors $\boldsymbol{E}_i^+$ and $\boldsymbol{E}_i^-$ are determined via (7) and, thus, $\boldsymbol{E}_r$ is calculated via (12).

Given the value of $\boldsymbol{E}_r$, we can analyze the capability of a magnetized plasma slab to act as a polarization converter. The following reflection coefficients:

$$\begin{cases} \Gamma_{\eta\eta} = E_{\eta,r}/E_{\eta,i} \\ \Gamma_{\zeta\eta} = E_{\zeta,r}/E_{\eta,i} \end{cases} \tag{18}$$

help quantify LP-to-LP conversion, as they are sufficient to describe the behavior of an η-axis polarized incident wave. In this case, the polarization conversion ratio (PCR) is defined as

$$\text{PCR} = \frac{|\Gamma_{\zeta\eta}|^2}{|\Gamma_{\zeta\eta}|^2 + |\Gamma_{\eta\eta}|^2}. \tag{19}$$

The PCR quantifies the amount of power transferred from the incident wave to its cross-polarized direction (i.e., the ζ-axis). At the same time, the parameter used to describe the LP-to-CP conversion is the axial ratio (AR), namely the ratio between the major and the minor axes of a generic polarization ellipse [32]. Conventionally, CP is defined for AR $\leq$ 3 dB [32].

B. Numerical Model

Numerical analyses have been accomplished with the commercial software CST microwave Studio[1]. The schematic of a simulated
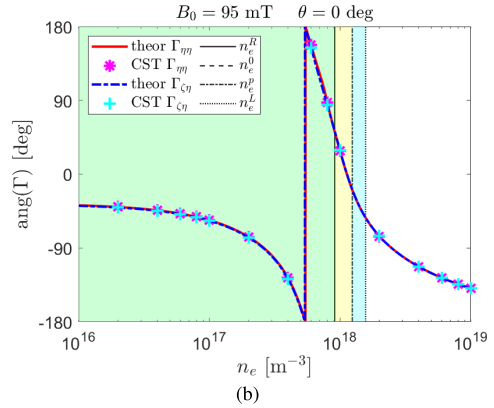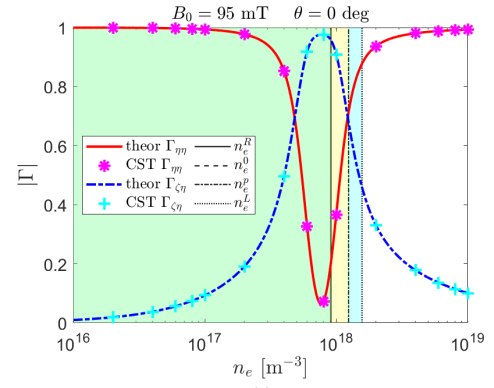
[1]Registered trademark.

(a)

(b)

Fig. 3. (a) Magnitude and (b) phase of the reflection coefficient Γ versus plasma density n_e. Both theoretical (theor) and numerical (CST) results are represented. The incident field is linearly polarized along η, $f = 10$ GHz, $z_{pl} = 0.7\lambda = 21$ mm, and $\nu = 3.1 \times 10^8$ Hz. Yellow, cyan, and green colors indicate the regions for which either *mode +*, *mode −*, or both *modes* propagate, respectively.

plasma element is depicted in Fig. 2. Its thickness is z_{pl}, the square plasma block measures $L_{pl} \times L_{pl}$, and the square ground plane is $L \times L$. The parameter L also represents the lattice periodicity [24]. The plasma is handled in CST via the native dispersion model called "Gyrotropic", conceived for media described by the anisotropic permittivity reported in (1); moreover, a generic direction of the magnetostatic field is allowed. Simulations rely on an unstructured tetrahedral mesh, where Maxwell's equations are solved in the frequency domain. As for the theoretical model, a linearly polarized plane wave is assumed to normally impinge the plasma element along the ξ-axis. Two simulations have been performed: 1) single-element analysis to verify the theoretical model and 2) array design to evaluate the capability of a plasma-based reflective surface to act as a polarization converter. The single element analysis is accomplished assuming Floquet boundary conditions along the η-axis and the ζ-axis; an open condition is imposed along the ξ-axis [24]. Moreover, $L = L_{pl}$ for consistency with the theoretical model, which refers to a slab geometry. Instead, open boundary conditions have been adopted along all directions to simulate the plasma-based reflective surface.

III. ELEMENT ANALYSIS

The theoretical model has been exploited to investigate the use of a magnetized plasma as a polarization converter, both LP-to-LP and LP-to-CP conversion have been considered. Numerical simulations have been performed to verify the theoretical model.

A. LP-to-LP Conversion

The considered plasma slab has thickness $z_{pl} = 21$ mm, i.e., 0.7λ at the central frequency $f = 10$ GHz. The LP-to-LP conversion is
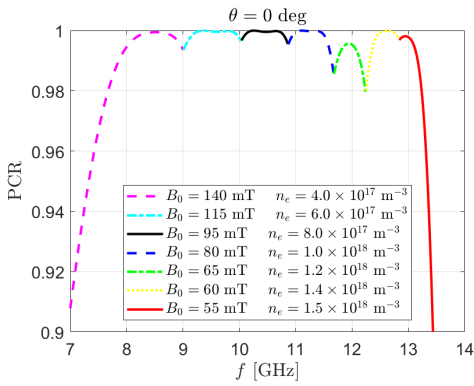
Fig. 4. PCR versus the operation frequency f for different combinations of plasma density n_e and magnetic field B_0. Here, the incident field is linearly polarized along η, $z_{pl} = 21$ mm, and $\nu = 3.1 \times 10^8$ Hz.

TABLE I
PLASMA PROPERTIES TO MAXIMIZE PCR AT $f = 10$ GHz

z_{pl} [mm]	B_0 [mT]	n_e [m^{-3}]	PCR
15	230	6.0×10^{17}	1.0
21	95	8.0×10^{17}	1.0
30	30	1.0×10^{18}	1.0

analyzed assuming the magnetostatic field with intensity $B_0 = 95$ mT and aligned with the ξ-axis, i.e., $\theta = 0°$. A neutral gas pressure $p_0 = 0.4$ mbar has been assumed for consistency with the plasma generation technology at the current state-of-the-art [2]. Without loss of generality, when the incident electric field is linearly polarized along the η-axis, the LP-to-LP conversion can be characterized via the $\Gamma_{\eta\eta}$, $\Gamma_{\zeta\eta}$, and PCR parameters defined in Section II-A.

The corresponding $\Gamma_{\eta\eta}$ and $\Gamma_{\zeta\eta}$ are depicted in Fig. 3 as a function of n_e for $L = L_{pl} = 15$ mm [24]. First, we can observe an excellent agreement between theoretical and numerical results (within an error $< 1\%$). Regarding the modulus of the reflection coefficient, $|\Gamma_{\eta\eta}|$ is minimum and $|\Gamma_{\zeta\eta}|$ is maximum in correspondence of $n_e = 8.0 \times 10^{17}$ m^{-3}. Here, PCR ≈ 1, meaning an almost complete cross-polarization conversion occurs. Instead, for $n_e \to 0$ or $n_e \approx 10^{19}$ m^{-3}, PCR $\to 0$, meaning the plasma does not affect the polarization. As a result, it is possible to rotate the LP in an arbitrary direction controlling n_e. The phase of the reflected wave is almost unaffected by the magnetostatic field, being practically the same as that produced by a non-magnetized plasma element [24]. Indeed, if $n_e \to 0$, the wave is almost not influenced by the presence of the plasma, and it is correspondingly reflected by the ground plane. If $n_e \approx 10^{19}$ m^{-3}, the plasma behaves itself as a good conductor, and the wave is reflected at the air-plasma interface with ang(Γ) $\approx -180°$. Intermediate situations are associated with different propagation paths within the plasma before the wave is reflected. Specifically, if $n_e \geq n_e^L$ only evanescent waves occur within the plasma, thus the EM propagation is almost entirely determined by the reflection at the air-plasma interface [24].

From a physical standpoint, the proposed LP-to-LP conversion relies on the Faraday rotation effect [27]. Namely, the two propagative *modes* occurring for $\theta = 0°$ are identified as R-waves and L-waves. The former is a right-handed CP wave propagating along the direction of the magnetostatic field, whilst the latter is a left-handed CP wave [27]. Being $u_+ \neq u_-$, the longer the path traveled by these two waves within the plasma before being reflected, the larger the rotation induced in the polarization direction. This is consistent with data reported in Fig. 3 since, for $n_e \lesssim n_e^R$, the Faraday rotation reaches its maximum before the R-wave becomes evanescent [27].

The capability of the proposed design to perform LP-to-LP conversion is analyzed in Fig. 4, where the operation frequency f
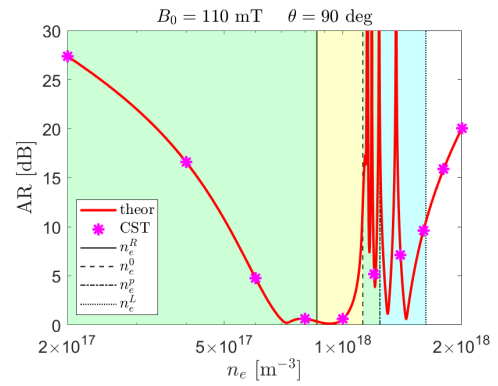

Fig. 5. AR versus plasma density n_e. Both theoretical (theor) and numerical (CST) results are represented. The incident field is linearly polarized at 45° in the η-ζ plane, $f = 10$ GHz, $z_{pl} = 0.7\lambda = 21$ mm, and $\nu = 3.1 \times 10^8$ Hz. Yellow, cyan, and green colors indicate the regions for which either *mode +*, *mode −*, or both *modes* propagate, respectively.
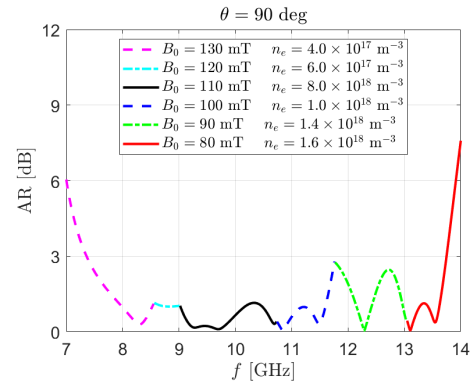

Fig. 6. AR versus operation frequency f for different combinations of plasma density n_e and magnetic field B_0. The incident field is linearly polarized at 45° in the η-ζ plane, $z_{pl} = 21$ mm, $\nu = 3.1 \times 10^8$ Hz.

varies. As one can note, cross-polarization conversion can take place over a remarkably large operation bandwidth (approximately from 7 to 13 GHz) by simply reconfiguring the plasma properties. Specifically, the relative bandwidth in which PCR ≥ 0.98 is 55% of the central frequency $f = 10$ GHz. It is worth noting that: 1) the condition $n_e \lesssim n_e^R$ is enforced by all the n_e and B_0 pairs reported in Fig. 4 and 2) the intensity of both n_e and B_0 are consistent with the plasma production technology at the current state-of-the-art [3], [26]. This confirms that the LP-to-LP conversion via plasma-based reflective surfaces is a feasible and appealing technology. Finally, Table I reports the plasma properties to achieve cross-polarization conversion at different values of z_{pl}. It is worth noting that the values of B_0 reported here are the minimum ones that allow achieving PCR ≈ 1.0 for at least one interval of n_e. In fact, the higher B_0, the higher the Faraday rotation effect [27]. By increasing too much B_0, the polarization direction might vary by more than 90°, which is out of the present scope. As one can note, the required intensity of B_0 is inverse proportional to z_{pl}. In particular, a slab thickness of $z_{pl} = 21$ mm is a trade-off between the compactness and the technological feasibility of the proposed design.

B. LP-to-CP Conversion

The same plasma slab analyzed in Section III-A is investigated in terms of LP-to-CP conversion. In this case, the magnetostatic field has intensity $B_0 = 110$ mT, and it is aligned with the ζ-axis, i.e., $\theta = 90°$. Moreover, the incident electric field is linearly polarized at 45° in the η–ζ-plane. The reflected wave is then analyzed in terms of circular polarization components through the parameter AR.
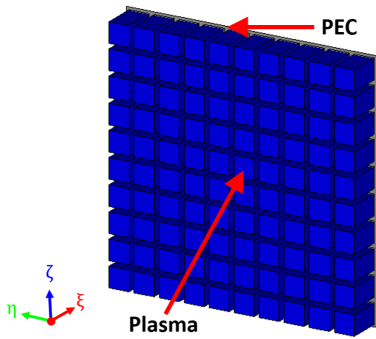
Fig. 7. Schematic of the plasma-based reflective surface. Each element is characterized by $L = 15$ mm, $L_{pl} = 12$ mm, and $z_{pl} = 21$ mm.

Fig. 5 shows the parameter AR as a function of n_e for the same plasma element described in Section III-A. Again, an excellent agreement is found between the theoretical and numerical results (within an error <1%). The condition AR ≤ 3 dB, which corresponds to an efficient LP-to-CP conversion, is achieved for n_e in the range 7.0×10^{17}–1.1×10^{18} m^{-3}. From a physical standpoint, this achievement is related to the wave *modes* excited by the incident electric field $\boldsymbol{E}_i$. The $E_{\zeta,i}$ component, parallel to $\boldsymbol{B}_0$, couples to an ordinary wave (O-wave). In contrast, the $E_{\eta,i}$ component, perpendicular to $\boldsymbol{B}_0$, couples to an extraordinary wave (X-wave) [27]. According to (8), O-the waves are associated with the *mode* + and X-waves with *mode* − [27]. Provided O-waves and X-waves are orthogonal [31], the CP condition is obtained for a 90° phase shift between Γ^+ and Γ^- and, in turn, between $E_{\zeta,r}$ and $E_{\eta,r}$. Moreover, it is possible to switch between the right-handed and left-handed CP by rotating $\boldsymbol{E}_i$ of 90° in the η–ζ plane. A more practical implementation of this feature (not envisioned by the theoretical model in its current form) is obtained by orienting $\boldsymbol{B}_0$ along the η-axis instead of the ζ-axis.

The proposed design is analyzed as the operation frequency f varies; see Fig. 6. By reconfiguring the plasma properties, a circularly polarized reflected wave is achievable in a large operation bandwidth (approximately from 7 to 14 GHz). Remarkably, the relative bandwidth for which AR ≤ 3 dB is 65% of the central frequency $f = 10$ GHz. The intensities of n_e and B_0 are consistent with the plasma production technology at the state-of-the-art [3], [26]. Therefore, this confirms that LP-to-CP conversion via a plasma-based reflective surface is feasible and appealing.

IV. ARRAY DESIGN

A design closer to practical implementation has been analyzed numerically to investigate further the feasibility of a plasma-based reflective surface with polarization conversion capabilities The setup is depicted in Fig. 7: it is composed of 10×10 plasma elements, each characterized by $L = 15$ mm, $L_{pl} = 12$ mm, and $z_{pl} = 21$ mm. The lattice periodicity is $L = 0.5\lambda$ at the central frequency $f = 10$ GHz [32]. The condition $L_{pl} = 0.8 \, L$ has been imposed to account for the additional equipment required to operate the array ensuring homogeneity and controllability of the plasma properties (e.g., vessels to confine the neutral gas and electrodes to ignite the discharge) [3].

The performance of the plasma-based reflective surface, in terms of PCR, is shown in Fig. 8 as the operating frequency is varied; here, $\theta = 0°$. It is confirmed that PCR ≥ 0.98 over a broad operation bandwidth, approximately 7–13 GHz. Concerning the theoretical model's results shown in Fig. 4, higher values of n_e are required to obtain similar outcomes consistently to what happens in nonmagnetized systems due to the presence of propagation paths outside the plasma medium [24]. Nonetheless, this is only a minor issue since the values of B_0 and n_e are still within feasible ranges for the plasma technology at the state-of-the-art [3], [26]. Similar considerations hold for AR,
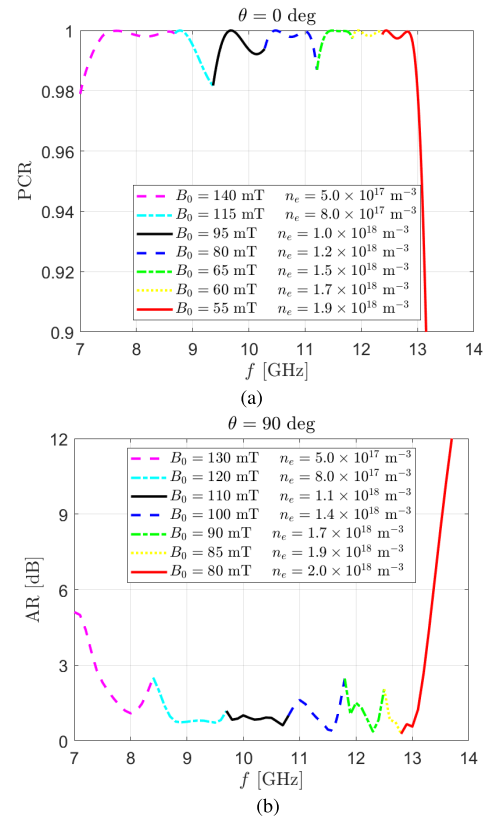

(a)

(b)

Fig. 8. (a)PCR and (b) AR versus operation frequency f for different combinations of plasma density n_e and magnetic field B_0. These data are obtained regarding the plasma-based reflective surface depicted in Fig. 7 and for $\nu = 3.1 \times 10^8$ Hz.

here computed for $\theta = 90°$. In this case, the operation bandwidth where AR ≤ 3 dB spans between 7.5 and 13 GHz. It is worth mentioning that the performance depicted in Fig. 8 is very close to the one derived from the reflection coefficients of each element of the reflective surface: differences are <0.01 in terms of PCR, and <0.1 dB in terms of AR. Similar results have also been obtained in the case of nonmagnetized systems [24], highlighting a generally mild cross-talking among plasma elements.

To sum up, given that 1) n_e is varied up to 2.0×10^{18} m^{-3} with a resolution of 1.0×10^{17} m^{-3}, 2) B_0 is varied in the range 55–140 mT, and 3) the direction of the magnetostatic field is changed over the ξ-axis, η-axis, and the ζ-axis, then the proposed plasma-based reflective surface enables:

1) the cross-polarization conversion;
2) LP-to-LP conversion for a generic polarization direction;
3) LP-to-CP conversion with the possibility to select between the right-handed and left-handed CP.

All these features are achievable from 7.5 to 13 GHz, namely, with a 55% relative bandwidth with respect to the central frequency $f = 10$ GHz, and for a fixed incident electric field. No other design proposed in the literature enables all these features in the GHz frequency range and for such a large operation bandwidth. Moreover, the requirements listed above are feasible with the plasma technology at state-of-the-art and assuming the magnetostatic field is generated with a suitable set of electromagnets [30].

V. CONCLUSION

A feasibility study has been accomplished to assess, for the first time, the use of reflective surfaces based on magnetized plasmas for polarization conversion. A theoretical model has been formulated to analyze LP-to-LP and LP-to-CP converters relying on this concept. Afterward, the numerical design of a plasma-based reflective surface

is presented. The latter enables 1) cross-polarization conversion, 2) generic LP-to-LP conversion, and 3) LP-to-CP conversion with the possibility to select between the right-handed and left-handed CP. To the best of the authors' knowledge, this is the first concept enabling all these features in the GHz range with a relative bandwidth larger than 50%. From a technological standpoint, it requires the plasma density to be controlled up to 2.0×10^{18} m^{-3}, and the magnetic field shall be varied in the range 55–140 mT with the possibility to change its direction along three perpendicular axes. The practical implementation of these constraints, while challenging, is entirely feasible. In fact, the controllability of the plasma density has been demonstrated in the field of GPAs [2], [10], and electromagnets providing variable magnetostatic fields up to 200 mT are commonly used in electric space propulsion [30].

In conclusion, the proposed solution is extremely appealing regarding polarization conversion capabilities. Thus, the realization and testing of a proof of concept will be the subject of future works. At the same time, a drawback of plasma-based reflective surfaces is their relative thickness, almost doubled with respect to other systems presented in the literature [18], [20]. Nonetheless, the most critical aspect that might hinder the applicability of these devices in realistic scenarios (e.g., intelligent reflecting surfaces—IRSs [33]) is the nonnegligible power consumption, in the range of several watts [3]. This drawback can be substantially mitigated by taking advantage of the recent technological advances made in the field of electric space propulsion in terms of optimization and miniaturization of the electronics to manage the plasma [26].

REFERENCES

[1] T. Anderson, *Plasma Antennas*. Norwood, MA, USA: Artech House, 2020.

[2] A. Daykin-Iliopoulos et al., "Characterisation of a thermionic plasma source apparatus for high-density gaseous plasma antenna applications," *Plasma Sources Sci. Technol.*, vol. 29, no. 11, Nov. 2020, Art. no. 115002.

[3] P. De Carlo, M. Magarotto, G. Mansutti, S. Boscolo, A.-D. Capobianco, and D. Pavarin, "Experimental characterization of a plasma dipole in the UHF band," *IEEE Antennas Wireless Propag. Lett.*, vol. 20, no. 9, pp. 1621–1625, Sep. 2021.

[4] T. Naito, S. Yamaura, Y. Fukuma, and O. Sakai, "Radiation characteristics of input power from surface wave sustained plasma antenna," *Phys. Plasmas*, vol. 23, no. 9, Sep. 2016, Art. no. 093504.

[5] P. De Carlo, M. Magarotto, G. Mansutti, A. Selmo, A.-D. Capobianco, and D. Pavarin, "Feasibility study of a novel class of plasma antennas for SatCom navigation systems," *Acta Astronautica*, vol. 178, pp. 846–853, Jan. 2021.

[6] N. Souhair, M. Magarotto, E. Majorana, F. Ponti, and D. Pavarin, "Development of a lumping methodology for the analysis of the excited states in plasma discharges operated with argon, neon, krypton, and xenon," *Phys. Plasmas*, vol. 28, no. 9, Sep. 2021, Art. no. 093504.

[7] M. Guaita, M. Magarotto, M. Manente, D. Pavarin, and M. Lavagna, "Semi-analytical model of a helicon plasma thruster," *IEEE Trans. Plasma Sci.*, vol. 50, no. 2, pp. 425–438, Feb. 2022.

[8] G. Mansutti et al., "Modeling and design of a plasma-based transmit-array with beam scanning capabilities," *Results Phys.*, vol. 16, Mar. 2020, Art. no. 102923.

[9] G. Mansutti et al., "Design of a hybrid metal-plasma transmit-array with beam-scanning capabilities," *IEEE Trans. Plasma Sci.*, vol. 50, no. 3, pp. 662–669, Mar. 2022.

[10] M. Magarotto et al., "Numerical suite for gaseous plasma antennas simulation," *IEEE Trans. Plasma Sci.*, vol. 49, no. 1, pp. 285–297, Jan. 2021.

[11] S. A. Winkler, W. Hong, M. Bozzi, and K. Wu, "Polarization rotating frequency selective surface based on substrate integrated waveguide technology," *IEEE Trans. Antennas Propag.*, vol. 58, no. 4, pp. 1202–1213, Apr. 2010.

[12] M. Wang and Z. Zhai, "Wide-angle circular polarization converter based on a metasurface of Z-shaped unit cells," *Frontiers Phys.*, vol. 8, Oct. 2020, Art. no. 527394.

[13] Q. Zheng, C. Guo, and J. Ding, "Wideband metasurface-based reflective polarization converter for linear-to-linear and linear-to-circular polarization conversion," *IEEE Antennas Wireless Propag. Lett.*, vol. 17, no. 8, pp. 1459–1463, Aug. 2018.

[14] L. Martinez-Lopez, R. Martinez-Lopez, J. Rodriguez-Cuevas, A. E. Martynyuk, and J. I. Martinez-Lopez, "A dual circularly-polarized multilayer reflective surface based on loaded ring slots," *IEEE Access*, vol. 9, pp. 6990–6999, 2021.

[15] W. Yang, K.-W. Tam, W.-W. Choi, W. Che, and H. T. Hui, "Polarisation rotation reflective surface based on artificial magnetic conductor and its application," *Electron. Lett.*, vol. 50, no. 21, pp. 1500–1502, Oct. 2015.

[16] M. I. Khan and F. A. Tahir, "A compact half and quarter-wave plate based on bi-layer anisotropic metasurface," *J. Phys. D, Appl. Phys.*, vol. 50, no. 43, 2017, Art. no. 43LT04.

[17] R. Zaker and A. Sadeghzadeh, "A low-profile design of polarization rotation reflective surface for wideband RCS reduction," *IEEE Antennas Wireless Propag. Lett.*, vol. 18, no. 9, pp. 1794–1798, Sep. 2019.

[18] B. Lin, L. Lv, J. Guo, Z. Liu, X. Ji, and J. Wu, "An ultra-wideband reflective linear-to-circular polarization converter based on anisotropic metasurface," *IEEE Access*, vol. 8, pp. 82732–82740, 2020.

[19] Y.-P. Li, H.-F. Zhang, T. Yang, T.-Y. Sun, and L. Zeng, "A multi-functional polarization converter base on the solid-state plasma metasurface," *IEEE J. Quantum Electron.*, vol. 56, no. 2, Apr. 2020, Art. no. 7300107.

[20] X. Gao, W. L. Yang, H. F. Ma, Q. Cheng, X. H. Yu, and T. J. Cui, "A reconfigurable broadband polarization converter based on an active metasurface," *IEEE Trans. Antennas Propag.*, vol. 66, no. 11, pp. 6086–6095, Nov. 2018.

[21] W. Li et al., "A reconfigurable polarization converter using active metasurface and its application in horn antenna," *IEEE Trans. Antennas Propag.*, vol. 64, no. 12, pp. 5281–5290, Dec. 2016.

[22] Y. Tian, X. Ai, Y. Han, and X. Liu, "Investigation on broadband propagation characteristic of terahertz electromagnetic wave in anisotropic magnetized plasma in frequency and time domain," *Phys. Plasmas*, vol. 21, no. 12, 2014, Art. no. 123303.

[23] S. Cho, "Scattering and polarization conversion of electromagnetic waves obliquely incident on a magnetized plasma layer," *Phys. Plasmas*, vol. 24, no. 7, Jul. 2017, Art. no. 073302.

[24] M. Magarotto, L. Schenato, P. De Carlo, and A.-D. Capobianco, "Feasibility of a plasma-based intelligent reflective surface," *IEEE Access*, vol. 10, pp. 97995–98003, 2022.

[25] H. A. E.-A. Malhat and S. H. Zainud-Deen, "Plasma-based artificial magnetic conductor for polarization reconfigurable dielectric resonator antenna," *Plasmonics*, vol. 15, no. 6, pp. 1913–1924, Dec. 2020.

[26] N. Bellomo et al., "Design and in-orbit demonstration of REGULUS, an iodine electric propulsion system," *CEAS Space J.*, vol. 14, no. 1, pp. 79–90, Jan. 2022.

[27] J. A. Bittencourt, *Fundamentals of Plasma Physics*. New York, NY, USA: Springer, 2004.

[28] D. Melazzi, V. Lancellotti, and A.-D. Capobianco, "Analytical and numerical study of a gaseous plasma dipole in the UHF frequency band," *IEEE Trans. Antennas Propag.*, vol. 65, no. 12, pp. 7091–7101, Dec. 2017.

[29] M. A. Lieberman and A. J. Lichtenberg, *Principles of Plasma Discharges and Materials Processing*. Hoboken, NJ, USA: Wiley, 2005.

[30] K. Takahashi, "Magnetic nozzle radiofrequency plasma thruster approaching twenty percent thruster efficiency," *Sci. Rep.*, vol. 11, 2021, Art. no. 2768.

[31] C. G. Someda, *Electromagnetic Waves*. Boca Raton, FL, USA: CRC Press, 2017.

[32] C. A. Balanis, *Antenna Theory: Analysis and Design*. Hoboken, NJ, USA: Wiley, 2015.

[33] Q. Wu, S. Zhang, B. Zheng, C. You, and R. Zhang, "Intelligent reflecting surface-aided wireless communications: A tutorial," *IEEE Trans. Commun.*, vol. 69, no. 5, pp. 3313–3351, May 2021.